Photo-Hall investigation of p-type HgTe-CdTe superlattices

C. A. Hoffman, J. R. Meyer, E. R. Youngdale, J. R. Lindle, and F. J. Bartoli
Naval Research Laboratory (Code 6551), Washington, D.C. 20375-5000

K. A. Harris, J. W. Cook, Jr., and J. F. Schetzina
Department of Physics, North Carolina State University, Raleigh, North Carolina 27695-8202
(Received 5 August 1987)

We discuss detailed transport and phototransport measurements on a p-type HgTe-CdTe superlattice grown by molecular-beam epitaxy (MBE). At low temperatures, the field-dependent Hall data indicate the presence of low-mobility carriers in addition to the high-mobility holes reported previously. Intrinsic electrons become evident at temperatures as low as 50 K. The temperature dependence of the intrinsic carrier density yields information concerning the band gap and the product of the electron and hole density-of-states effective masses. Photo-Hall measurements were also performed using high-intensity irradiation from a CO_2 laser to generate excess electrons and holes. From these measurements, we obtain the first determination of minority-carrier mobilities in Hg-based superlattices. At 10 K, the minority electron mobility is found to be slightly lower than that of the majority holes. Free-carrier lifetimes have been studied by three independent techniques: photo-Hall analysis, transient-decay measurements, and photoconductive response. The lifetime is found to be on the order of 1 ns.

I. INTRODUCTION

In a number of previous studies,[1-5] the photo-Hall technique has been used to characterize a wide range of material properties in narrow-gap semiconductors. Majority and minority carrier mobilities, linear and nonlinear free-carrier lifetimes, donor and acceptor concentrations, impurity binding energies, electron-hole scattering, and the dynamic Burstein shift have been investigated in both n- and p-type samples of the $Hg_{1-x}Cd_xTe$ alloy. Here we report the first application of this technique to narrow-band-gap Hg-based superlattices.

Following a brief description of the molecular-beam-epitaxy (MBE) sample growth in Sec. II, Sec. III discusses the dark-Hall measurements and analysis. Consideration of the magnetic field dependence of the Hall coefficient at each temperature allows one to account for mixed-conduction effects and to determine the densities and mobilities of individual carrier species. Photo-Hall measurements and analysis reported in Sec. IV are shown to yield a characterization of the minority-carrier mobility. The photo-Hall data also provide a characterization of the free-carrier lifetime as a function of temperature. This is discussed in Sec. V along with lifetimes obtained by two other methods, photoconductive decay and photoconductive response. A further result of the photo-Hall investigation, concerning which of the various carrier species coexist in the superlattice, is used in Sec. VI in analyzing the intrinsic carrier density data. The experimental temperature dependence of n_i yields a nonoptical characterization of the superlattice band gap, as well as the product of the electron and hole density-of-states effective masses.

II. MBE SUPERLATTICE GROWTH

The HgTe-CdTe superlattice was prepared at North Carolina State University in an MBE system designed and built specifically for growing Hg-based films and multilayers. The system consists of a preparation and analysis chamber, a main MBE growth chamber, and a load lock for introducing and retrieving samples from either chamber. The main flange on the growth chamber has provisions for seven MBE source ovens with computer-controlled shutters for multilayer-film growth. The source flange also serves as the base for an internal cryoshroud which continuously maintains the shroud at cryogenic temperatures whenever Hg is in the system. Because large Hg vapor flux densities at the substrate are required for film growth, a special Hg MBE source was designed and constructed. This source is equipped with platinum resistance thermometers to ensure superior temperature stability (± 0.05 °C at 200 °C).

The HgTe-CdTe superlattice (52–52 Å) was deposited onto a (100) CdTe substrate which had been chemimechanically polished and etched prior to its use. After the substrate was transferred into the MBE growth chamber, a 2-μm-thick buffer layer of CdTe was first deposited at 275 °C using the MBE effusion source containing high-purity CdTe. The substrate temperature was then lowered to 175 °C and alternating layers of HgTe-CdTe were deposited. The entire superlattice was grown with the Hg source shutter open such as to generate a constant Hg flux density at the substrate, corresponding to a beam equivalent pressure of about 2×10^{-4} Torr. Rather than being pure CdTe, the barrier layers are therefore composed of the $Hg_{1-x}Cd_xTe$ alloy, with x es-

timated to be in the range 0.85–0.90. The Te and CdTe source shutters were opened and closed sequentially at preselected times in a cyclic fashion for the growth of HgTe and CdTe layers, respectively. The final superlattice thickness was 2 μm.

III. DARK-HALL MEASUREMENTS AND ANALYSIS

Van der Pauw Hall measurements have been performed as a function of magnetic field (up to 5 kG) and temperature (10 to 300 K). At each B and T, these data yield a "measured" carrier density

$$n_m(B)=1/eR_H \tag{3.1}$$

and a "measured" mobility

$$\mu_m(B)=\sigma(B=0)/n_m(B)e\ , \tag{3.2}$$

where R_H and σ are the experimental Hall coefficient and conductivity, respectively. For a fixed magnetic field of 1 kG, Figs. 1 and 2 give the observed temperature dependences of n_m and μ_m. Qualitatively, these data indicate that the sample is p type (since the Hall coefficient is positive at low temperatures) with a hole mobility of at least 10^4 cm^2/V s.[6] However, at temperatures as low as 60 K the intrinsic electron density becomes high enough to reverse the sign of R_H.

Most semiconductor transport results are reported in terms of measurements at a single magnetic field, such as those illustrated by Figs. 1 and 2. As long as only one type of carrier is present, n_m and μ_m represent good approximations to the density and mobility of the carrier (to within the Hall factor r_H). However, in this as well as all other type-III p-type Hg-based superlattice samples we have examined thus far,[7] mixed conduction by at least two carrier species is evident at all temperatures. Conclusions based on the Hall measurements at a single magnetic field can therefore be quite misleading. Much more information can be extracted if the magnetic field dependence of the Hall coefficient and conductivity are measured and a more comprehensive analysis performed.

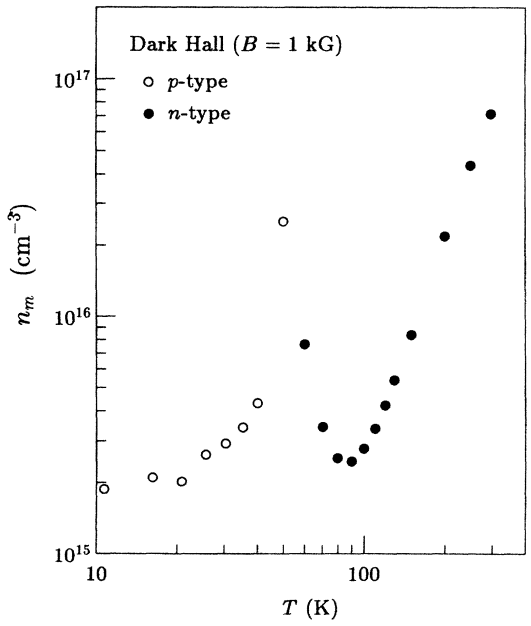

FIG. 1. Measured (dark) carrier density vs temperature at a fixed magnetic field of 1 kG.

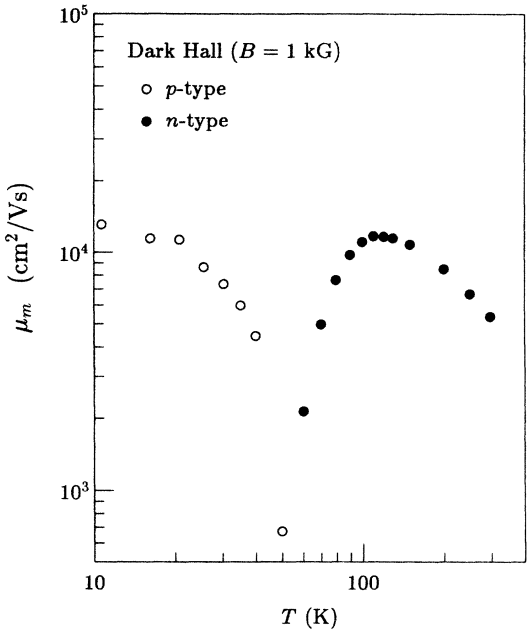

FIG. 2. Measured (dark) mobility vs temperature at a fixed magnetic field of 1 kG.

For the present sample we find that at least three types of carriers are needed to account for the data in various temperature regions: a high-mobility electron, a high-mobility hole (p_1) similar to that reported previously,[6] and an additional low-mobility carrier whose charge could not be determined. Although we will assume for definiteness that the low-mobility carrier is a hole (p_2), care will be taken to assure that this assumption does not affect the conclusions reached below.

If we assume there are three carriers and employ a simplified model in which a discrete mobility is associated with each, the mixed-conduction expressions for the conductivity and Hall coefficient may be written[8]

$$\sigma(B=0)=\sigma_{xx}(B=0)=ne\mu_n+p_1e\mu_{p1}+p_2e\mu_{p2}\ , \tag{3.3}$$

$$R_H(B)=\frac{\sigma_{xy}/B}{\sigma_{xx}^2+\sigma_{xy}^2}\ , \tag{3.4}$$

where the xx and xy components of the conductivity tensor are given by

$$\sigma_{xx}(B)=\frac{ne\mu_n}{1+\mu_n^2B^2}+\frac{p_1e\mu_{p1}}{1+\mu_{p1}^2B^2}+\frac{p_2e\mu_{p2}}{1+\mu_{p2}^2B^2}\ , \tag{3.5}$$

$$\sigma_{xy}(B)=-\frac{ne\mu_n^2B}{1+\mu_n^2B^2}+\frac{p_1e\mu_{p1}^2B}{1+\mu_{p1}^2B^2}+\frac{p_2e\mu_{p2}^2B}{1+\mu_{p2}^2B^2}\ . \tag{3.6}$$

Least-squares fits of the above expressions to the Hall and conductivity data have been performed to obtain temperature-dependent densities and mobilities for the electron and two types of holes.

Since the sample is p type, no electrons are observed at low temperatures ($T<40$ K). However, mixed conduction by both the high-mobility hole and the low-mobility carrier is evident. The analysis is fairly sensitive to the mobility of the high-mobility hole μ_{p1} (the uncertainty is estimated to be less than 20%), but slightly less sensitive to its density $p_1 \approx (3\pm1.0)\times10^{14}$ cm^{-3}. Because the maximum magnetic field employed in the present study did not exceed 5 kG (our current investigations employ B up to 70 kG), the analysis is able to specify only the product $p_2\mu_{p2}$ rather than the density and mobility of the low-mobility carrier independently. The estimated lower bound on p_2 is 2×10^{16} cm^{-3}, which implies $\mu_{p2}\leq 700$ cm^2/V s.

The temperature dependence of μ_{p1} is given by the triangles of Fig. 3. (Above 50 K, the data are not sensitive enough to allow reliable values to be obtained.) Note that the actual low-temperature mobility μ_{p1} is nearly a factor of 3 larger than the value implied by the unreduced data in Fig. 2. It should also be pointed out that down to 10 K, no peak is observed in μ_{p1}, as would be expected if ionized impurity scattering were dominant. The pronounced decrease of μ_{p1} with T in the range 20–50 K is considerably more abrupt than would be expected due to phonon scattering. The mobility μ_{p2}, also obtained from the fit, is nearly constant below 50 K. At higher temperatures, it begins a relatively mild decrease with increasing T.

At temperatures as low as 50 K, the data begin to show evidence for intrinsic electrons. When $T\geq 70$ K, reliable electron mobilities can be obtained, which are given by the open circles in Fig. 3. (The photo-Hall μ_n shown as the solid circles will be discussed below.) The decrease of μ_n with increasing temperature is in qualitative agreement with what one expects from phonon scattering. Also obtained from the dark-Hall analysis is the intrinsic electron density, which will be discussed below in Sec. VI.

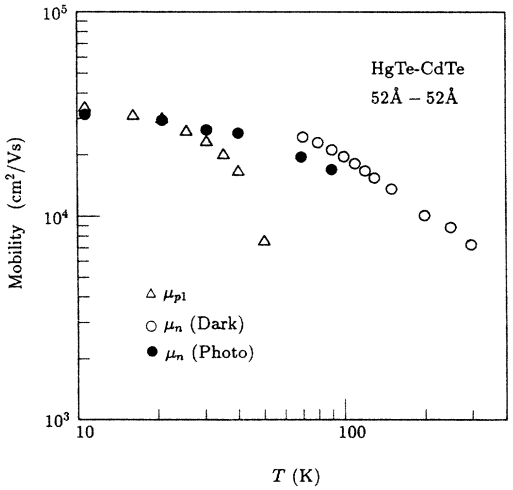

FIG. 3. Experimental electron and p_1 hole mobilities. Open circles (electrons) and triangles (holes) were derived from the mixed-conduction analysis of the dark-Hall data while the solid circles (electrons) were obtained from the photo-Hall analysis.

IV. PHOTO-HALL MEASUREMENTS AND ANALYSIS

The photo-Hall apparatus employed in the present investigation was described previously in Ref. 1. The sample is mounted in a variable temperature refrigerator and placed between the pole pieces of an electromagnet, which provides uniform magnetic fields up to 5 kG. The photo-Hall measurements are made using a Transiac transient digitizer which is interfaced to a MicroVax computer for immediate data storage and processing. Optical excitation is provided by a CO_2 laser, operating at 9.27 μm, and externally shuttered to produce 25-μs flat-top pulses. The laser intensity on the sample is varied by means of calibrated attenuators. Uniform illumination is assured by requiring that the focused spot size of the incident radiation be large compared to the sample. Illumination intensities are measured so that the dependence of excess carrier density on laser flux can be determined.

If the photoexcitation level is varied at a given temperature and magnetic field, the measured mobility μ_m versus measured density n_m traces out a curve, whose functional form is governed by the mixed-conduction expressions discussed above [Eqs. (3.1)–(3.6)]. In order to understand the data, it is useful to first consider the simpler problem in which there is only one type of hole. We also assume (1) low temperatures, for which $n\approx 0$ in the absence of optical excitation, (2) $\Delta n=\Delta p$, i.e., no trapping, and (3) the electron and hole mobilities do not depend on Δn.[9] Using the low-field forms of Eqs. (3.5) and (3.6) (which are applicable to the photo-Hall measurements at 500 G discussed below), one obtains in the low-excitation limit

$$\sigma_{xx}\approx\sigma^0_{xx}\left[1+\frac{\Delta n}{p^0}\left[\frac{\mu_n}{\mu_p}+1\right]\right], \tag{4.1}$$

$$\sigma_{xy}\approx\sigma^0_{xy}\left[1+\frac{\Delta n}{p^0}\left[-\frac{\mu_n^2}{\mu_p^2}+1\right]\right], \tag{4.2}$$

where quantities labeled with a superscript "0" represent the values in the absence of photoexcitation ($\Delta n=0$). From these relations, one easily finds the measured density and mobility to be

$$n_m\approx n^0_m\left[1+\frac{\Delta n}{p^0}\left[\frac{\mu_n}{\mu_p}+1\right]^2\right], \tag{4.3}$$

$$\mu_m\approx\mu^0_m\left[1-\frac{\Delta n}{p^0}\frac{\mu_n}{\mu_p}\left[\frac{\mu_n}{\mu_p}+1\right]\right]. \tag{4.4}$$

Combining the two equations by eliminating $\Delta n/p^0$ yields

$$\mu_m\approx\mu^0_m\left[1-\left[\frac{n_m}{n^0_m}-1\right]\left[\frac{\mu_n}{\mu_n+\mu_p}\right]\right] \tag{4.5}$$

from which we may find the derivative of the μ_m versus n_m curve

$$s \equiv \frac{d(\mu_m/\mu_m^0)}{d(n_m/n_m^0)} = -\frac{\mu_n}{\mu_n+\mu_p} . \tag{4.6}$$

The slope of the curve may have values between -1 and 0, depending on μ_n/μ_p.[10] In order to exploit this sensitivity to the mobility ratio as a technique for characterizing the minority electron mobility, it is useful to invert Eq. (4.6) so that μ_n is expressed in terms of the experimentally determined value of s and the μ_p known from the dark-Hall data

$$\mu_n = \frac{(-s)\mu_p}{1+s} . \tag{4.7}$$

We now return to the more complicated case in which two different types of holes are present. The most straightforward assumption is that both are coexistent in the superlattice. For $p_2 \gg p_1$ it follows that $\Delta p_2 \gg \Delta p_1$ in quasiequilibrium, since the density of states is much larger in the p_2 band. With the relations $\Delta p_2 \approx \Delta n$, $\Delta p_1 \approx (p_1/p_2)\Delta n$, and $p_1\mu_{p1}^2 > p_2\mu_{p2}^2$, the three-carrier generalization of Eq. (4.7) becomes

$$\mu_n = \frac{(-2s-1)\mu_{p1}}{(1+s)(p_2\mu_{p2}/p_1\mu_{p1}+1)} . \tag{4.8}$$

It will be seen below in Fig. 4 that the photo-Hall data at 10 K yield $s \approx -0.4$. However, Eq. (4.8) shows that a negative electron mobility is obtained in fitting any s greater than -0.5. Furthermore, in the present example one obtains an unreasonably low electron mobility for any s greater than ≈ -0.7. We conclude that the data cannot be fit if one assumes $\Delta p_2 \approx \Delta n$ and that both types of holes coexist.

We therefore consider the possibility that the two types of holes do not coexist and that $\Delta p_1 \approx \Delta n$ ($\Delta p_2 \approx 0$). One then finds

$$s = -\frac{\mu_n^2(p_1\mu_{p1}+p_2\mu_{p2})+\mu_n p_1\mu_{p1}^2-p_2\mu_{p2}\mu_{p1}^2}{\mu_n^2(p_1\mu_{p1}+p_2\mu_{p2})+2\mu_n p_1\mu_{p1}^2-p_2\mu_{p2}\mu_{p1}^2+p_1\mu_{p1}^3} \tag{4.9}$$

which reduces to Eq. (4.6) if $p_2\mu_{p2}=0$. Without explicitly giving the inversion for μ_n as a function of s, we simply note that the final term in the numerator considerably reduces the magnitude of the negative slope if $\mu_{p2} \approx \mu_n$. (Under some circumstances s may become positive.)

The open circles of Fig. 4 show the curve traced out by the measured mobility versus measured carrier density at $B=500$ G and $T=10$ K. The Hall coefficient is positive (p type), and the measured carrier density increases with increasing Δn. Also shown are results of the mixed-conduction analysis, where minority-electron mobility is the only fitting parameter. In obtaining these curves, we used $\Delta p_1 = \Delta n$ and did not allow the mobilities to vary with photoexcitation, but made none of the other simplifying assumptions employed in obtaining expressions (4.1)–(4.9). As predicted in the qualitative discussion above, the slope of the curve is found to be quite sensitive to the minority electron mobility. The best fit at 10 K is obtained for $\mu_n \approx 3.2\times10^4$ cm^2/V s, with an experimental uncertainty of less than 20%. (Improper assumptions going into the analysis could naturally make the error much larger.)

Figure 4 also shows results at $T=40$ K, which are similarly sensitive to the electron mobility. Note that here the photoexcitation is nearly strong enough to drive the Hall coefficient through crossover to n-type behavior. When this occurs n_m increases to infinity, then decreases again as a negative density.

Figure 5 shows data and analysis for somewhat higher temperatures, where n_m in the absence of photoexcitation is already n-type due to the presence of intrinsic electrons. At 70 K, the holes dominate σ_{xx}^0 while the electrons dominate σ_{xy}^0. This condition leads to the double-valued behavior exhibited by both the data and the analytical curve. This shape is quite similar to that observed previously for p-type bulk $Hg_{1-x}Cd_xTe$ at intermediate temperatures (see Ref. 3, Fig. 5). The present analysis predicts that at high photoexcitation levels ($n \approx p_1$ and $n\mu_n \gg p_2\mu_2$) the measured mobility should approach a constant value governed by mixed conduction between the electrons and p_1 holes.

When T is increased to 90 K, both σ_{xx}^0 and σ_{xy}^0 are dominated by intrinsic electrons. The dark-Hall data then become less sensitive to hole densities and mobilities, which are needed as input to the photo-Hall analysis. For this reason, the photo-Hall electron mobilities and lifetimes (discussed below) have much higher uncertainty when the temperature is above $\approx$90 K.

The filled circles of Fig. 3 show the temperature dependence of minority-electron mobilities obtained from the

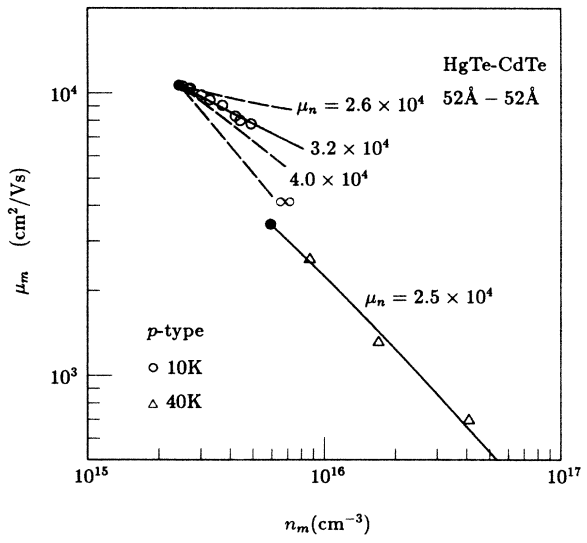

FIG. 4. Measured mobility vs measured carrier density from photo-Hall data (points) and analysis (curves) at 10 and 40 K. The solid circles represent data in the absence of photoexcitation. The magnetic field was 500 G, and all data showed a positive Hall coefficient (p type).

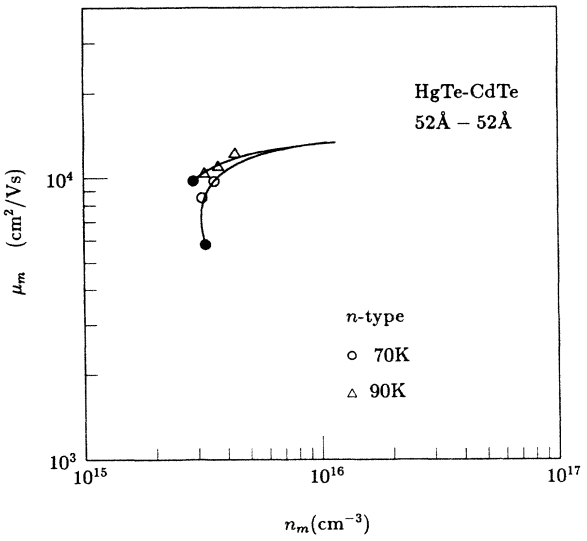

FIG. 5. Measured mobility vs measured carrier density from photo-Hall data (points) and analysis (curves) at 70 and 90 K. The solid circles represent data in the absence of photoexcitation. The magnetic field was 500 G and all data showed a negative Hall coefficient (n type).

photo-Hall analysis. It is encouraging that even though the dark-Hall coefficients cross from p type to n type and pass from a region where $n^0 \approx 0$ to one where the intrinsic electrons dominate both σ_{xx}^0 and σ_{xy}^0, the photo-Hall mobilities form a smooth curve which joins the dark-Hall curve. The discrepancy between the open and solid circles is only $\approx 25\%$ at 70 K. It is noteworthy that the photo-Hall mobilities are nearly independent of temperature at low T, rather than decreasing as would be expected if ionized impurity scattering (by impurities in the wells) dominated. Although this type of behavior is observed in n-type bulk $Hg_{1-x}Cd_xTe$, in that case it is attributable to degeneracy of the electron population at low temperatures.[11] For the same reason, it should not be surprising that the electron mobilities in n-type HgTe-CdTe superlattices generally have little temperature dependence at low T.[12] However, at low excitation levels for which the minority electron population is nondegenerate, the mobility in p-type bulk $Hg_{1-x}Cd_xTe$ decreases as T is decreased from 20 to 10 K.[3] The absence of a low-temperature decrease in the p-type superlattice, therefore, raises questions about scattering by ionized impurities in the wells being the dominant mechanism for electrons at low temperatures.

V. LIFETIME STUDIES

The free-carrier lifetime in the superlattice was studied by three different methods: (1) photo-Hall analysis, (2) photoconductive decay, and (3) photoconductive response.

When the photo-Hall data are analyzed as discussed in the previous section, the electron mobility is derived from a fit to the μ_m versus n_m curve. Once the best mobility has been obtained, Eqs. (3.1)–(3.6) may be solved for the excess electron density corresponding to each photo-Hall data point. [For example, the simplified expression (4.3) may easily be inverted to give Δn as a function of n_m.] Results at 10, 40, 70, and 90 K as a function of laser photon density Φ are shown in Fig. 6, where the solid lines correspond to a linear dependence of Δn on Φ. We find that the lifetime is nearly linear at these excitation levels.

If the absorption coefficient α is also known, one may estimate the magnitude of the free-carrier lifetime

$$\tau = \frac{\Delta n}{(1-R)\Phi(1-e^{-\alpha t})/t} , \tag{5.1}$$

where R is the reflectivity and t is the thickness of the superlattice. Although α has not been determined for the present sample, we can at least estimate its value by comparing with the small amount of absorption data which has been published thus far. In particular, we consider Fig. 3 of Patten *et al.*,[13] which gives $\alpha(\hbar\omega)$ at 300 K for a superlattice with 61 Å HgTe wells and 25 Å CdTe barriers. Since these data were taken for conditions not exactly corresponding to those of present interest, we also need to estimate the shift of the band edge with layer thicknesses and temperature. To accomplish this, we have employed the theoretical band structure model of Schulman and Chang.[14] At 10 K we estimate that the temperature shift of the band edge approximately cancels the shift due to the smaller well thickness in the present sample. At a laser wavelength of 9.27 μm we then obtain $\alpha(10\text{ K}) \approx 800\text{ cm}^{-1}$. However, at higher temperatures, the gap is expected to increase, and we estimate $\alpha(70\text{ K}) \approx 450\text{ cm}^{-1}$. Substituting into Eq. (5.1) yields photo-Hall lifetimes given by the open circles in Fig. 7. While the dip at 20 K may not be statistically significant, the increase in τ at higher temperatures is clearly indicated by the data. Results at temperatures above 70 K have not been included because of the larger uncertainties in the

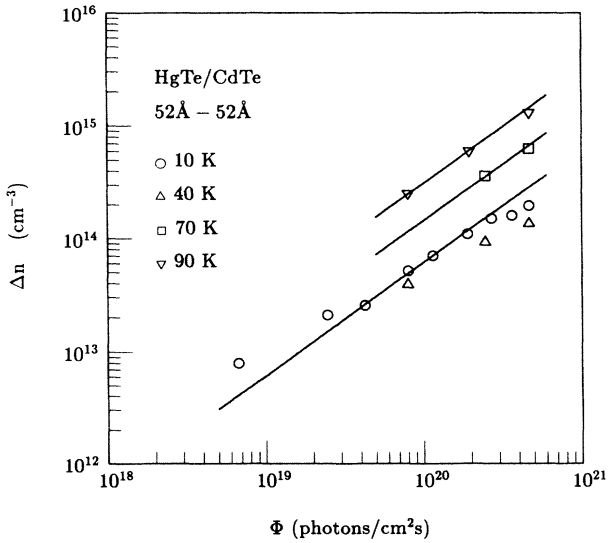

FIG. 6. Excess electron density vs laser photon density from the photo-Hall analysis. The solid lines correspond to a linear dependence.

photo-Hall analysis in that region (see the discussion of this point in Sec. IV).

The second method for determining lifetimes consisted of measuring the transient decay of the photoconductivity due to 1.5 ns pulses from a Nd:YAG laser operating at 1.06 μm. Although the lifetimes were too short for a highly-accurate determination to be possible, rough estimates could at least be made from the rise and fall times of the photoconductivity signal. Results are shown for the solid circles of Fig. 7. To within expected uncertainties, the agreement between photoconductivity and photo-Hall lifetimes is quite good. This would appear to provide further evidence that the interpretation of the photo-Hall data, as discussed in Sec. IV, is essentially correct.

The third method involved measuring the photoconductive response due to chopped radiation from a cw $Ga_xAl_{1-x}As$ diode laser operating at 0.8 μm. The relative change in conductivity is given by

$$\frac{\Delta\sigma}{\sigma^0}=\frac{\Delta ne(\mu_n+\mu_{p1})}{\sigma^0}=\frac{f(1-R)\eta P_0\tau(\mu_n+\mu_{p1})}{\hbar\omega t n_m^0\mu_m^0}\ , \tag{5.2}$$

where $f\approx 0.287$ is a form factor to account for the triangular shape of the pulses, P_0 is the laser power density, and the temperature-dependent electron and hole mobilities are taken from the dark- and photo-Hall results. For the quantum efficiency we arbitrarily chose the temperature-independent value $\eta\approx 3$, although uncertainty in this parameter considerably increases the potential error in the magnitude of the lifetime. The triangles of Fig. 7 represent the temperature-dependent lifetimes obtained from the photoconductive response data using this expression. Although the temperature dependence is similar to that found by the photoconductive decay method, the magnitude is as much as a factor of 10 higher. The photoconductive-decay results should probably be considered the more reliable since that method is more direct, and a lifetime of 10 ns would have been easily resolvable in the transient signal.

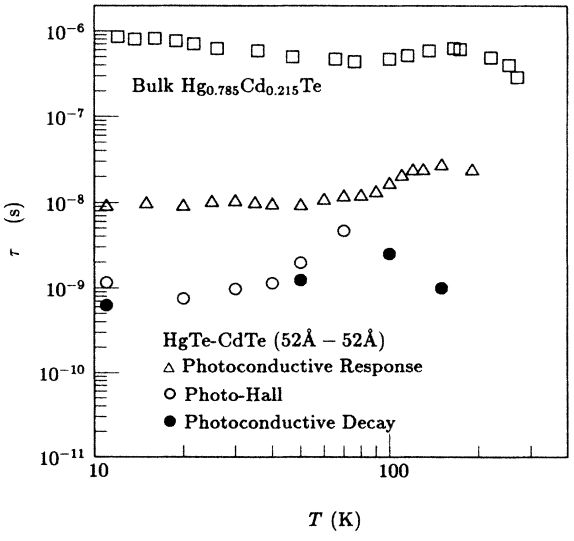

FIG. 7. Free-carrier lifetimes vs temperature for p-type bulk $Hg_{1-x}Cd_xTe$ and the p-type HgTe-CdTe superlattice. The superlattice lifetime was determined by three different methods.

For comparison, the boxes in Fig. 7 represent temperature-dependent lifetimes in p-type bulk $Hg_{1-x}Cd_xTe$.[15] Although the temperature dependences of superlattice and bulk are similar, the lifetime in the superlattice is nearly 3 orders of magnitude shorter. In the alloy, the decreasing τ at high temperatures is due to Auger recombination. However, Auger recombination in the superlattice would have to be over 2 orders of magnitude stronger than in the alloy for that process to account for the high-temperature decrease observed in both the photoconductive decay and photoconductive response data.

VI. INTRINSIC CARRIER DENSITY

In this section we use the densities n obtained from the Hall data to analyze the intrinsic carrier density n_i as a function of temperature. Although the superlattice band structure is expected to be extremely nonparabolic,[14] we may to a first approximation consider the conventional "law of mass action" result.[16] Assuming nondegenerate statistics and parabolic bands,

$$n_i^2=np=4\left[\frac{k_BT}{2\pi\hbar^2}\right]^3(m_n^{ds}m_p^{ds})^{3/2}e^{-E_g/k_BT}\ , \tag{6.1}$$

where the density-of-states electron and hole effective masses must be averaged over parallel and perpendicular directions, i.e., $m_i^{ds}\approx m_{\parallel}^{2/3}m_{\perp}^{1/3}$. Note that if a linear variation of the energy gap with temperature is introduced, $E_g(T)=E_g^0+\Gamma(T/300)$, where E_g^0 is the gap at zero temperature and Γ is the normalized temperature coefficient, the functional dependence of n_i on T is unchanged and only the multiplicative constant is altered.

Since the Hall analysis gives n rather than n_i, the intrinsic density obtained is sensitive to the value assumed for the hole density p. In Sec. IV it was found that while one cannot account for the photo-Hall data if the total valence-band density of states is assumed to be dominated by the low-mobility (p_2) holes, the results appear quite consistent if the photoexcitation is assumed to produce primarily electrons and high-mobility (p_1) holes. This implies that the intrinsic electrons should also be accompanied primarily by high-mobility rather than low-mobility holes. Taking

$$p=n+N_A-N_D\approx n+p_1(T=0)$$

in Eq. (6.1), one obtains the intrinsic carrier density versus inverse temperature given by the open circles of Fig. 8. In this figure n_i has been normalized by $T^{3/2}$ so that the parabolic law of mass action is given by a straight line. The open circles are in fact found to closely follow a straight line over the temperature range 90–300 K. However, at lower temperatures the data lie above the line, by an amount which is larger than the estimated uncertainty in the experiment and analysis. This may be due to nonparabolicity of the conduction and valence

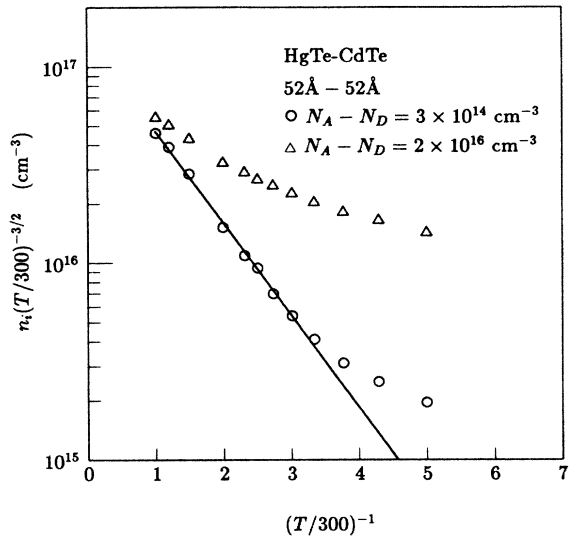

FIG. 8. Intrinsic carrier density (normalized by $T^{3/2}$) vs inverse temperature, as determined from the dark-Hall data. Intrinsic densities n_i were obtained from the electron densities n using two different values for $N_A - N_D$. The solid curve is the best straight line through the data for $N_A - N_D = 3.0 \times 10^{14}$ cm^{-3}.

bands.[17] For comparison, the triangles of Fig. 8 show the intrinsic density one obtains assuming $N_A - N_D \approx p_2(T=0)$, where the lower bound has been used for p_2. While the fact that the triangles fail to follow a straight line anywhere does not automatically rule out their being correct, the photo-Hall results argue against using $N_A - N_D \approx p_2$.

From the slope of the line in Fig. 8, Eq. (6.1) allows one to estimate the zero-temperature extrapolation of the energy gap. The result is

$$E_g^0 \approx 56 \text{ meV} \tag{6.2}$$

which is considerably smaller than the value 119 meV calculated from the calculation of Schulman and Chang[14] using $x = 0.9$ (rather than pure CdTe) in the barriers and -40 meV for the valence band offset.[18] On the other hand, if -350 meV is used for the valence band offset,[19–21] the calculation gives 70 meV, which is a much better agreement. This is contrary to the case of the adsorption data reported by Patten *et al.*,[13] whose features agreed better with theoretical results employing the smaller valence band offset. In the near future an attempt will be made to perform photo-Hall and absorption characterizations on the same samples. The Hall data clearly show evidence for intrinsic electrons at temperatures as low as 50 K, which is far below where they are observable, for example, in $Hg_{0.2}Cd_{0.8}Te$.

Equation (6.1) also shows that from the magnitude of the straight line in Fig. 8, one may calculate the product of the electron and hole density-of-states effective masses. Using the calculation of Schulman and Chang to estimate the temperature coefficient of the gap $\Gamma \approx 80$ meV, we obtain

$$(m_e^{ds} m_h^{ds})^{1/2} \approx 0.087 m_0 \ . \tag{6.3}$$

Although this is approximately a factor of 2 higher than the product in $Hg_{0.8}Cd_{0.2}Te$, it must be remembered that the perpendicular masses are factored into the density-of-states average. Since $m_\perp$ is expected to be quite large for hole bands,[14] our result implies small parallel masses for both electrons and holes. The value $m_{ds} \approx 0.087 m_0$ is in good agreement with a rough theoretical estimate obtained using the formalism of Schulman and Chang at the top of the valence band and the bottom of the conduction band (with -350 meV for the valence band offset). In a future study, the large nonparabolicity of the dispersion relations will be included in a detailed calculation of the intrinsic carrier density, in order to verify whether the experimental temperature dependence of n_i is reproduced.

We finally note that electron densities taken directly from the unreduced Hall data at a single magnetic field (Fig. 1) would have been far too inaccurate to be used in the type of analysis discussed in this section. Magnetic-field-dependent measurements are required so that mixed-conduction effects may be eliminated.

VII. CONCLUSIONS

We must still address the question of why the Hall data show evidence for at least two types of holes, while only p_1 appears to be generated when excess electrons are excited optically. As discussed above, the finding implies that the two holes are not coexistent in the same part of the sample. One possibility is that the p_2 holes are not in the superlattice at all, but on the surface or at some interface, e.g., between the superlattice and the substrate. The two-dimensional density would then be at least $\approx 4 \times 10^{12}$ cm^{-2}, which is somewhat high but not out of the question. Another possibility is that the superlattice is nonuniform in the growth direction, with holes at different layers having different densities and mobilities. Such a nonuniformity could result, for example, from strain originating in the substrate or from interdiffusion during the growth process, which would be less extensive in the top layers not exposed to the high temperatures for as long. As was stated in Ref. 7, the observation of more than one type of hole at low temperatures is not specific to the particular superlattice discussed here. If the low-mobility carrier is an electron rather than a hole, it seems probable that it exists at a surface or interface rather than within the superlattice. It would then not be surprising that the low-mobility carrier is not affected by photoexcitation.

Finally, we summarize the accomplishments of the present work. Dark-Hall measurements were performed and analyzed to obtain electron and hole densities and mobilities for a broad temperature range. At low temperatures a low-mobility carrier is observed in addition to the high-mobility hole reported previously, and it is found to be necessary to consider mixed conduction at all temperatures. Photo-Hall measurements have also been

performed as a function of temperature and laser intensity. It is shown that the "measured" mobility versus "measured" density curves are quite sensitive to the minority-electron mobility. The data are inconsistent if it is assumed that most of the photoexcited holes go into the more numerous low-mobility states. However, if the photoexcited holes are assumed to be of the high-mobility type, then the minority-electron mobilities obtained from the photo-Hall analysis join smoothly to those obtained from the dark-Hall data in the intrinsic range. The photo-Hall experiment also yields free-carrier lifetimes, which are consistent with those obtained from transient photoconductivity measurements. Lifetimes estimated from photoconductive response measurements were somewhat higher. Consideration of the intrinsic carrier density as a function of temperature leads to a characterization of the zero-temperature energy gap as well as the product of the electron and hole density-of-states effective masses.

We have demonstrated that magnetic-field and temperature-dependent Hall measurements as well as temperature- and intensity-dependent photo-Hall measurements provide powerful tools for probing the free-carrier properties at the bottom of the conduction band and top of the valence band in narrow-gap superlattices.

ACKNOWLEDGMENTS

The authors are grateful to J. Schulman for allowing the use of his HgTe-CdTe superlattice band structure software in estimating temperature and barrier and/or well thickness dependences of the band gap.

[1]C. A. Hoffman, F. J. Bartoli, and J. R. Meyer, J. Appl. Phys. **61**, 1047 (1987).

[2]J. R. Meyer, F. J. Bartoli, and C. A. Hoffman, J. Vac. Sci. Technol. A **5**, 3035 (1987).

[3]F. J. Bartoli, C. A. Hoffman, and J. R. Meyer, J. Vac. Sci. Technol. A **4**, 2047 (1986).

[4]F. J. Bartoli, J. R. Meyer, C. A. Hoffman, and R. E. Allen, Phys. Rev. B **27**, 2248 (1983).

[5]F. Bartoli, R. Allen, and M. Kruer, J. Appl. Phys. **45**, 2150 (1974).

[6]High hole mobilities in HgTe–CdTe superlattices were first reported by J. P. Faurie, M. Boukerche, S. Sivananthan, J. Reno, and C. Hsu, Superlatt. Microstruct. **1**, 237 (1985). See also J. P. Faurie, IEEE J. Quantum Electron. **QE-22**, 1656 (1986).

[7]At this writing, we have examined five type-III *p*-type Hg-based superlattices, three grown by J. F. Schetzina and co-workers and two grown by J. P. Faurie and co-workers. All showed mixed conduction by at least two types of carriers at low temperatures. In two, both carriers were clearly holes, in one there was one electron and one hole (whose densities increased with temperature in a manner suggesting that they were intrinsic down to 4.2 K), and in the other two (including the present sample) there was one hole and one low-mobility carrier whose sign could not be determined.

[8]A. C. Beer, *Galvanomagnetic Effects in Semiconductors* (Academic, New York, 1963), Sec. 12.

[9]Although this is known not to be a good assumption for $Hg_{1-x}Cd_xTe$ alloys at high excitation levels (see Refs. 1–4), it is probably reasonable at the relatively low Δn of interest here.

[10]In *p*-type bulk $Hg_{1-x}Cd_xTe$, $\mu_n/\mu_p > 100$ so $s \approx -1$ in Fig. 5 of Ref. 3.

[11]J. R. Meyer, F. J. Bartoli, and C. A. Hoffman, in *Proceedings of the 7th International Conference on Ternary and Multinary Compounds*, edited by S. K. Deb and A. Zunger (Materials Research Society, Pittsburgh, 1987), p. 559.

[12]K. A. Harris, S. Hwang, J. W. Blanks, J. W. Cook, Jr., J. F. Schetzina, and N. Otsuka, J. Vac. Sci. Technol. A **4**, 2061 (1986).

[13]E. A. Patten, K. Kosai, T. N. Casselman, J. N. Schulman, Y.-C. Chang, and J.-L. Staudenmann, J. Vac. Sci. Technol. A **5**, 3102 (1987).

[14]J. N. Schulman and Y.-C. Chang, Phys. Rev. B **33**, 2594 (1986).

[15]S. E. Schacham and E. Finkman, J. Appl. Phys. **57**, 2001 (1985).

[16]For example, see C. Kittel, *Introduction to Solid State Physics* (Wiley, New York, 1971), p. 368.

[17]For example, a dependence qualitatively like that observed may result if the effective mass is smaller at the top of the highest valence band than it is farther down. Such behavior has been obtained theoretically in Ref. 14.

[18]Y. Guldner, G. Bastard, J. P. Vieren, M. Voos, J. P. Faurie, and A. Million, Phys. Rev. Lett. **51**, 907.

[19]S. P. Kowalczyk, J. T. Cheung, E. A. Kraut, and R. W. Grant, Phys. Rev. Lett. **56**, 1605 (1986).

[20]Tran Minh Duc, C. Hsu, and J. P. Faurie, Phys. Rev. Lett. **58**, 1127 (1987).

[21]S.-H. Wei and A. Zunger, Phys. Rev. Lett. **59**, 144 (1987).